JGR Space Physics

RESEARCH ARTICLE
10.1029/2020JA028747

Key Points:

- During geomagnetic storms, Joule heating enhances thermospheric density at remote poleward (higher) latitudes
- The latitude/LT difference between peak Joule heating and peak density enhancement increases/shortens as storm intensifies
- heating, more important in affecting density, has the better correlation with density discrepancy for more intense storms

Correspondence to:
J. Miao and S. Liu,
miaoj@nssc.ac.cn;
liusq@nssc.ac.cn

Citation:
Wang, X., Miao, J., Lu, X., Aa, E., Liu, J., Wang, Y., & Liu, S. (2021). Latitudinal impacts of Joule heating on the high-latitude thermospheric density enhancement during geomagnetic storms. *Journal of Geophysical Research: Space Physics*, *126*, e2020JA028747. https://doi.org/10.1029/2020JA028747

Received 1 OCT 2020
Accepted 15 APR 2021

Latitudinal Impacts of Joule Heating on the High-Latitude Thermospheric Density Enhancement During Geomagnetic Storms

Xin Wang[1,2,3], Juan Miao[1,3], Xian Lu[4], Ercha Aa[1,3], Ji Liu[5], Yuxian Wang[1,2], and Siqing Liu[1,2,3]

[1]National Space Science Center, Chinese Academy of Sciences, Beijing, China, [2]College of Earth and Planetary Sciences, University of Chinese Academy of Sciences, Beijing, China, [3]Key Laboratory of Science and Technology on Environmental Space Situation Awareness, CAS, Beijing, China, [4]Department of Physics and Astronomy, Clemson University, Clemson, SC, USA, [5]Department of Physics, University of Alberta, Edmonton, Canada

Abstract We investigate the thermosphere latitudinal response to Joule heating from 265 geomagnetic storms during the period of January 2002 to December 2008. The total mass density enhancements at 400 km are derived from the Challenging Minisatellite Payload (CHAMP) and the Gravity Recovery and Climate Experiment (GRACE) satellites with temporal and spatial coverage. We examine Joule heating and its influence on the thermospheric density using data from the Defense Meteorological Satellite Program (DMSP) spacecraft and Weimer-2001 electric potential model for storms. The results show that during geomagnetic storms, Joule heating can cause the thermospheric density to enhance in the higher-latitude areas. In addition, during weak and moderate geomagnetic storms, the difference in the latitude corresponding to strong Joule heating with the latitude where high-latitude thermospheric density enhances is only 0°–10° latitudes, while increases to 10°–15° for the intense storms. Besides, it is found that the peak density enhancement in LT is closer to peak Joule heating for more intense geomagnetic storms.

1. Introduction

Solar-terrestrial energy has a crucial influence on the composition and dynamics of the high-latitude thermosphere (Prölss, 2011; Richmond & Lu, 2000). The thermosphere is affected fundamentally through solar extreme ultraviolet (EUV) radiation and magnetospheric energy input. EUV energy input is the dominant driver in quiet time, but for high-latitude thermosphere during geomagnetic storms, magnetospheric energy can far exceed it (Knipp et al., 2004; Prölss, 2011). Furthermore, Joule heating and particle precipitation are the two main forms of magnetospheric energy, while during geomagnetic storms Joule heating can count for up to two-thirds of the energy being deposited into the thermosphere (Knipp et al., 2004). During the most active times, the mechanism of injection energy transfer from the solar wind to the coupled magnetosphere-ionosphere-thermosphere (CMIT) system is ultimately dissipated into the thermosphere through strong Joule heating (Deng et al., 2011; Lu et al., 2016; Shi et al., 2017; Wu et al., 2020).

Joule heating arises from the exchange of energy and momentum between the plasma and the neutral thermosphere. During the geomagnetic storm, solar wind brings tremendous energy into magnetosphere-ionosphere-thermosphere system, and intensifies Joule heating in the high-latitude regions (Buonsanto, 1999; Sutton et al., 2009), which heats the neutral thermosphere to expand upwards (Wilson et al., 2006). As a result, the whole thermosphere circulates, and rises through the large-scale gravity waves and neutral wind surges, leading to the global thermospheric density disturbance (Emmert, 2015; Fuller-Rowell et al., 1994; Wu et al., 2020). Besides, the neutral wind in thermosphere is driven by Coriolis forces, ion-neutral drag forces, and solar pressure gradients (Rishbeth, 1977), while Coriolis forces play the fundamental role in effecting neutral wind (Forbes & Roble, 1990; Hagan & Sipler, 1991; Zhang et al., 2015).

The variation of total mass density can influence thermospheric dragging force, resulting in the decay of Low Earth Orbit (LEO) satellites with time. Consequently, human space activity such as the identification, lifetime, and spacecraft maneuver can be affected (Emmert, 2015; Krauss et al., 2018; Zesta & Huang, 2016). The prediction of the thermospheric density variability associated with thermospheric drag is still a central

topic for space weather application. Several empirical thermospheric models contribute greatly to the determination of thermospheric density (Doornbos & Klinkrad, 2006; Hedin, 1987, 1991; Jacchia, 1971), while the most widely utilized and researched model in application for satellite orbit prediction is US Naval Research Laboratory Mass Spectrometer and Incoherent Scatter Radar Extended (NRLMSISE-00) (Picone et al., 2002), used to derive the thermospheric density with inputs of the F10.7 index, Ap index, Universal Time, and Location.

During the geomagnetic storm, energy injects from solar wind to magnetosphere-thermosphere system, affecting thermospheric density strongly. The LEO satellites are surrounded by the increasing neutral density, and experience tracking loss and satellites orbit decay with time (Oliveira & Zesta, 2019; Zesta & Huang, 2016). However, the NRLMSISE-00 model underestimates the thermospheric density during the active time, while the density discrepancies between observations and simulations reach the maximum (Wang, Miao, Liu, et al., 2020). To improve the capability of NRLMSISE-00 model of storm-time thermospheric density, it's necessary to investigate the relationship between energy injection by Joule heating and density discrepancy which represents the difference between the observations and model results during geomagnetic storms. Fedrizzi et al. (2012) found that Joule heating from the coupled thermosphere-ionosphere-plasmasphere electrodynamics (CTIPe) model can better estimate thermospheric density enhancement provided by empirical models. Wu et al. (2020) found that enhanced Joule heating at high latitudes can generally improve the model simulation in neutral densities compared with Gravity Recovery and Climate Experiment (GRACE) observations.

Therefore, the impacts of Joule heating on thermospheric density is critical to explore high-latitude density enhancement during geomagnetic storms. By the CMIT model, B. Zhang et al. (2012) concluded that Joule heating increases in the F region, leading to the density enhancement in high latitudes. Deng et al. (2013) discovered that during geomagnetic storm, the increased Joule heating can enhance the high-latitude thermospheric density by 24% at 400 km altitude. In addition, such an enhancement effect induced by Joule heating is latitude dependent. Barth et al. (2009) discovered that Joule heating in the 55°N–60°N latitude region causes the increase of the peak temperature of the thermosphere in the 60°N–75°N region. By using Thermosphere Ionosphere Mesosphere Electrodynamics General Circulation Model (TIME-GCM), Crowley et al. (2010) found that simulated Joule heating leads to the density enhancements comparable with the Challenging Minisatellite Payload (CHAMP) observations during the geomagnetic storm, and the latitude of the peak Joule heating is different from that of the peak thermospheric density. Thus, the differences between the peak Joule heating latitudes and those for the peak thermospheric density enhancements in the high-latitude areas are significant, which makes it worthwhile to investigate the impacts of Joule heating on the latitudinal distribution of thermospheric density responses during geomagnetic storms.

We follow the analysis methodology performed in Wang, Miao, Aa, et al. (2020), who provided the thermospheric density response times to Joule heating during geomagnetic storms through the statistical analysis of CHAMP and GRACE satellite observations and Joule heating calculations for 265 geomagnetic storms. In this study, we provide the same storm cases for thermospheric density and Joule heating but for the impacts of Joule heating on the latitudinal distribution of high-latitude density enhancement. Besides, we explore distribution of density discrepancy between observation and NRLMSISE-00 simulation, and the relationship of this distribution with Joule heating and the density enhancement.

Vickrey et al. (1982) found that Joule heating ($\sigma_P\,(\boldsymbol{E}+\boldsymbol{u}\times\boldsymbol{B})^2$) can be obtained by Pedersen conductivity (σ_P), the electric field ($\boldsymbol{E}$), the neutral wind ($\boldsymbol{u}$), and the geomagnetic field ($\boldsymbol{B}$). The electric field dominates Joule heating, while the impacts of neutral wind on Joule heating are intricate. In general, neutral winds make a significant contribution of Joule heating during weak geomagnetic storms and quiet time (Billett et al., 2018). We statistically analyze Joule heating by neglecting the neutral winds during geomagnetic storms for this study and we will examine Joule heating, including neutral wind, for a follow-on study.

The study is organized as follows: the data sources are described in Section 2. A detailed introduction to the thermospheric density enhancement is performed in Section 3. Joule heating and its influence on the high-latitude thermospheric density enhancement and density discrepancy for a single storm are presented in Section 4.1. The statistical analysis following the case study in Section 4.1 is performed in Section 4.2. Finally, we conclude with a summary and discussion in Section 5.

2. Data Sources

The Joule heating is calculated as discussed in Wang, Miao, Aa, et al. (2020). We use height-integrated Pederson conductance (Σ_p) and the electric field ($\boldsymbol{E}$) to examine the distribution of height-integrated Joule heating ($\Sigma_p \boldsymbol{E}^2$) and follow the outlined approach:

1. The Pederson conductance is mainly controlled by the solar radiation and particle precipitation. We obtain the particle precipitation conductance from Robinson et al. (1987) and calculate the solar radiation conductance by Robinson and Vondrak (1984). In this study, we use statistical patterns of auroral particle precipitation based on the different levels of geomagnetic storms to estimate height-integrated particle precipitation conductance (Hardy et al., 1987; Robinson et al., 1987), which can be expressed as

$$\Sigma_{p(elec)} = \frac{40E_0}{16 + E_0^2}\sqrt{I}, \tag{1}$$

   where E_0 and I are the average energy of particle precipitation and electron integral energy flux. These two data are statistically accumulated from the three satellites of SSJ/5 series (F16-F18) in DMSP spacecraft during 2010–2014 (Redmon et al., 2017).
2. The electric field $\boldsymbol{E}$ is obtained from Weimer-2001 electric potential model (Weimer, 2001). The Weimer-2001 model is an improved model of the electric potential with the input of solar wind conditions, IMF orientations, and Earth's dipole tilt. This model results include influences of substorm activities on night-side processes in the magnetotail

Different levels of geomagnetic storms can bring different magnitude changes to thermosphere. We characterize different geomagnetic storms as weak, moderate, and intense, based on the magnitude of the Disturbance storm-time index (Dst) and analyze hundreds of storms. The Dst is a measurement for the variation of global equatorial ring current, which is determined by the Earth's horizontal magnetic field. We follow Srivastava and Venkatakrishnan (2004) and Gonzalez et al. (1999) in defining the geomagnetic storm by its most negative Dst during the storm main phase.

In this study, we summarize the Dst range for each storm category, as well as the number of storms in each category during 2002–2008. The strongest category has the smallest number of storms. The ranges of the Dst index are $-49 < \text{Dst} \leq -30$ nT, $-99 < \text{Dst} \leq -50$ nT, and $\text{Dst} \leq -100$ nT for weak, moderate, and intense geomagnetic storms, respectively. In addition, 123 weak, 103 moderate and 39 intense storms are statistically analyzed.

3. Thermospheric Density Enhancement at High Latitudes

During geomagnetic storms, we use accelerometers onboard the CHAMP (Reigber et al., 2002) and GRACE (Tapley et al., 2004) satellites to study the temporal and spatial high-latitude thermospheric density enhancement. The CHAMP and GRACE satellites were both launched in a near-circular orbit with the inclination of 87.25° and 89.5°, respectively. Lühr et al. (2004), Rentz (2009), and Lühr and Marker (2013) have analyzed the CHAMP and GRACE satellites observations of the thermospheric density enhancements at high latitudes.

Furthermore, due to the near-circular orbits of CHAMP and GRACE satellites, the height of the satellite varies at different latitude regions in the orbit (Xu et al., 2011). Thus, the height variations of the satellites contribute to the variations of the thermospheric density data. To remove the differences in neutral densities caused by the varying heights of the satellite orbit, we used NRLMSISE-00 model to normalize both CHAMP and GRACE data to a constant height of 400 km, following the method of Liu et al. (2007) and Xu et al. (2015):

$$\rho\left(h_{400}\right) = \frac{\rho\left(z\right) \times \rho_M\left(h_{400}\right)}{\rho_M\left(z\right)}, \tag{2}$$

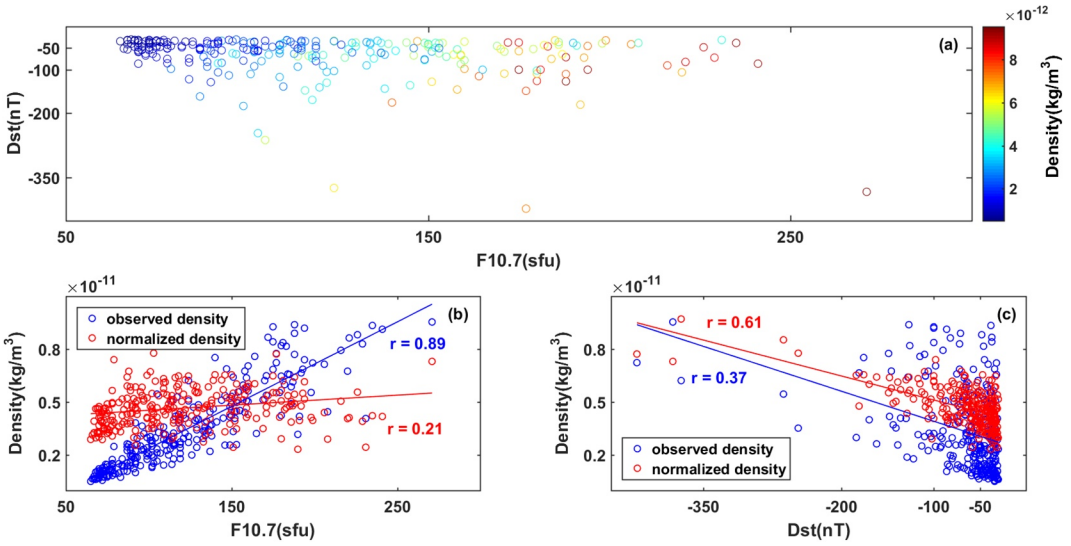

Figure 1. (a) The observed CHAMP daily averaged thermospheric density versus daily solar flux proxy F10.7, and Dst during 265 geomagnetic storm cases, (b) scatterplot and linear regression between F10.7 and the observed density (blue), the normalized density (red), (c) scatterplot and linear regression between Dst and the observed density (blue) and the normalized density (red). The blue and red lines are the fitting lines for observed density and normalized density, respectively. CHAMP, Challenging Minisatellite Payload.

where $\rho(h_{400})$ is the thermospheric density at a normalized height h_{400}, $\rho(z)$ is the CHAMP or GRACE observed density at the satellite orbit height z, and ρ_M is the corresponding neutral mass density obtained from the NRLMSISE-00 model.

Figure 1 shows that CHAMP daily averaged density varies with F10.7 and Dst from 265 geomagnetic storms. F10.7 and Dst are the proxies of solar radiation and geomagnetic activity. From Figure 1a, we can find that the observed thermospheric density increases with F10.7 and Dst. As shown in Figure 1b (blue line), the correlation coefficient (r) between observed density and F10.7 is 0.89. Thus, the quasi-linear correlation between density and F10.7 can be clearly found.

Solar radiation and geomagnetic activity are two fundamental impact factors on thermosphere, especially, affecting the variations in the thermospheric density (Lei et al., 2008; Liu & Lühr, 2005; Thayer et al., 2008). Thus, to better explore the impacts of magnitude of geomagnetic storms on thermospheric density, we need to exclude the influence of different solar radiation level on density. By roughly assuming that the density varies with F10.7 quasi-linearly, we normalize the solar radiation level to 150 sfu, which is the median value of solar radio flux for 265 geomagnetic storms, as Miao et al. (2012):

$$\rho(F_{150}) = \frac{\rho_M(F_{150})}{\rho_M(F)} \times \rho(F), \tag{3}$$

where $\rho(F_{150})$ is the thermospheric density at a normalized solar radiation F_{150}, $\rho(F)$ is the observed density at the measured solar radiation F, and ρ_M is the corresponding density obtained from the NRLMSISE-00 model.

After the normalization (Figure 1b, red line), from the smaller correlation coefficient, 0.21, between the density and F10.7, we can find that the dependence of neutral density on F10.7 becomes much weaker. In addition, after removing the solar cycle effects, density variation with Dst becomes less spread and irregular (Figure 1c, red line) than before the normalization (Figure 1c, blue line). By doing so, the impact of fluctuating solar radiation on thermospheric density is largely removed.

We define the storm-time thermospheric density enhancement as the difference between the density in the quiet time (Dst > −30 nT) and that in geomagnetically active condition. Although the NRLMSISE-00 model results underestimate the thermospheric density during geomagnetic storms, they agree reasonably well

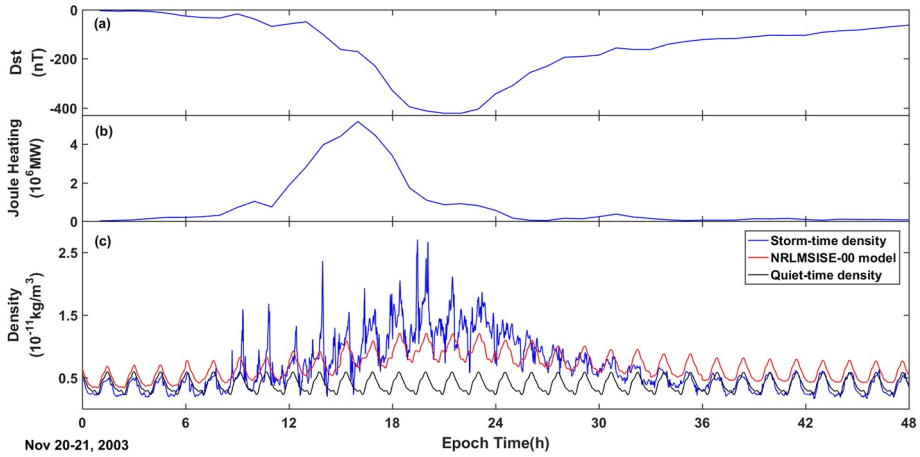

Figure 2. (a) Dst, (b) total Joule heating, and (c) thermospheric density observed from the CHAMP satellite (blue line), simulated by the NRLMSISE-00 model (red line) during November 20 and 21, 2003, compared with the prediction of the NRLMSISE-00 in the quiet time (black line). CHAMP, Challenging Minisatellite Payload.

with the observed density in the quiet time (Picone et al., 2002). Since the satellite did not pass the same locations during two adjacent days and the pure observations from the previous quiet day are relatively sparse, the density calculated by the NRLMSISE-00 model in the quiet time is taken as a reference to obtain storm-time thermospheric density enhancement. The daily Ap indices in the quiet time before the geomagnetic storms are used as the model input to obtain the quiet-time thermospheric densities.

4. Results

4.1. Storm Event of November 20 and 21, 2003

On November 20 and 21, 2003, solar wind impacted the magnetosphere-ionosphere-thermosphere system causing an intense geomagnetic storm, with Dst reaching −422 nT. Figure 2 shows the temporal variations of Dst, total Joule heating, the density measurements from CHAMP, and the density simulated by the NRLMSISE-00 model during this event. The total Joule heating is obtained from integrating the global distribution of Joule heating. The quiet-time densities are obtained from the NRLMSISE-00 model using the Ap index on November 19, 2003, which is before the onset of this event. The Dst index decreases significantly at 13 h, reaching the minimum at about 21 h, while Joule heating starts to increase around 11 h, peaking around 16 h. The densities from both observation and simulation mainly increase at about 14 h and peak at 20 h, concentrated on the main phase of geomagnetic storm, while the densities lag Joule heating by about 4 h. The NRLMSISE-00 results simulate the density evolution during the geomagnetic storm reasonably well, but underestimates the storm-time density during storm main phase, especially the peak observation.

Due to the limited spatial coverage by satellites, we accumulate observed densities per 3 h from all three satellites (CHAMP, GRACE-A, and GRACE-B). We assume that the density changes between successive orbits are progressive; thus, linear interpolation can be used to obtain the density lying between adjacent orbits. When the orbits from the three satellites have overlapped with each other, the averaged density is used for the grid with 0.25° × 0.25°. Such interpolation method has been used to study in the previous work (Wang, Miao, Aa, et al., 2020). We acquire the Joule heating from the methods introduced in Section 2, and calculate the 3-h average for Joule heating distribution corresponding to per 3 h thermospheric density. Finally, the obtained Northern Hemispheric distributions of Joule heating and thermospheric densities are shown in Figure 3 for the storm event of November 20, 2003. For the regions that observations are very sparse and linear interpolation fails to fill up the gaps, the areas are left blank.

Figures 3a–3d show the Northern Hemispheric pattern of Joule heating at 1200–1500 UT, 1500–1800 UT, 1800–2100 UT, and 2100–2400 UT, and Figures 3e–3h and 3i–3l show similar patterns of thermospheric density enhancement and density discrepancy. The gray circles are the satellite orbits of CHAMP and GRACE passing by. The density enhancement equals to the difference between the observations on November 20

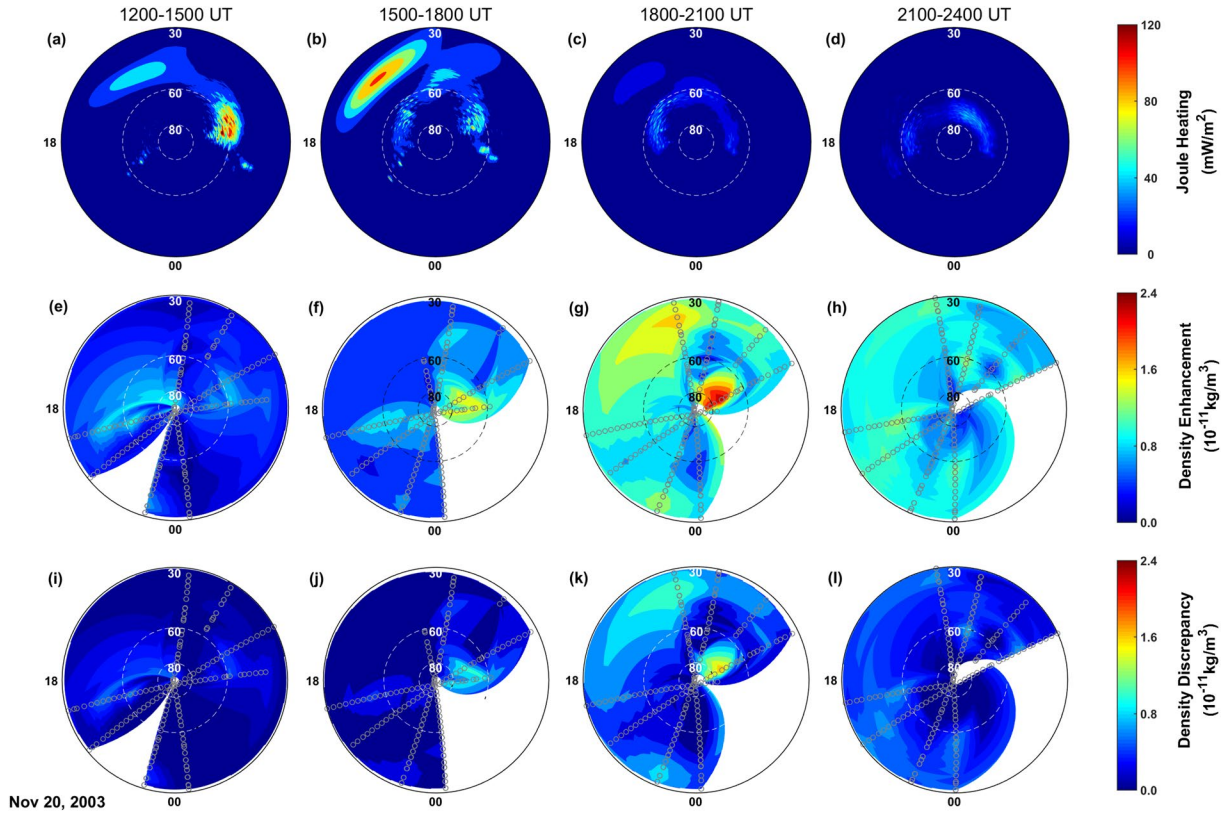

Figure 3. Intense geomagnetic storm event of November 20, 2003. (a–d) 3-h averaged height-integrated Joule heating, (e–h) thermospheric density enhancement, and (i–l) thermospheric density discrepancy during November 20, 2003, at 1200 —1500 UT, 1500–1800 UT, 1800–2100 UT, and 2100–2400 UT, respectively. The gray circles are the satellite orbits of CHAMP and GRACE passing by. The patterns are plotted in latitude versus local time coordinates, with the center of the pattern corresponding to the North Pole. The outside ring is 30°N and the bottom of ring is 00 LT.

(storm time) and the model results on November 19 (quiet time), and the density discrepancy represents the difference between the observations and model results both on November 20.

During the geomagnetic storm on November 20, 2003, Joule heating increases to peak in the high latitude area at 50°N–60°N, 0700–0900 LT at 1200–1500 UT (Figure 3a), and then it increases in the middle latitudes (40°N, 1400–1600 LT) at 1500–1800 UT (Figure 3b). The thermospheric density enhancement is concentrated on the high latitudes at 60°N–80°N, 0700–0900 LT at 1500–1800 UT (Figure 3f), where the density discrepancy appears obviously (Figure 3j). Subsequently, the density enhancement peaks at 1800–2100 UT in the cusp region with 75°N, 0800–0900 LT (Figure 3g), which has about 15° latitude difference and the same LT with the peak Joule heating at high latitudes (Figure 3a). The lag time that density delays Joule heating has also seen in Figures 2b and 2c. At the same time, the density discrepancy reaches the maximum in the area where the peak value of density enhancement is mainly concentrated (Figure 3k). Compared with the Joule heating in the middle latitudes (Figure 3b), the density enhancement increases at 40°N, 1300–1400 LT at 1800–2100 UT (Figure 3g). After that, Joule heating gradually reduces at 2100–2400 UT, while the density enhancement and the density discrepancy decrease compared with 1800–2100 UT.

By comparing Figures 3a and 3b with Figures 3f and 3g, the latitudes with the maximum thermospheric density enhancements are ~15° more poleward than those corresponding to the maximum Joule heating. Nevertheless, these two maxima have similar LT distribution (centered around 0700–0900 LT) during the intense geomagnetic storm. The response of storm-time thermospheric density lags Joule heating by about 3 h, as shown by the close spatial correlation between Figures 3a and 3g. Furthermore, the model results underestimate the high-latitude thermospheric density. Due to the influence of Joule heating, the density discrepancy increasing with the density enhancement is mainly concentrated on the high latitudes where the density enhancement and Joule heating peak.

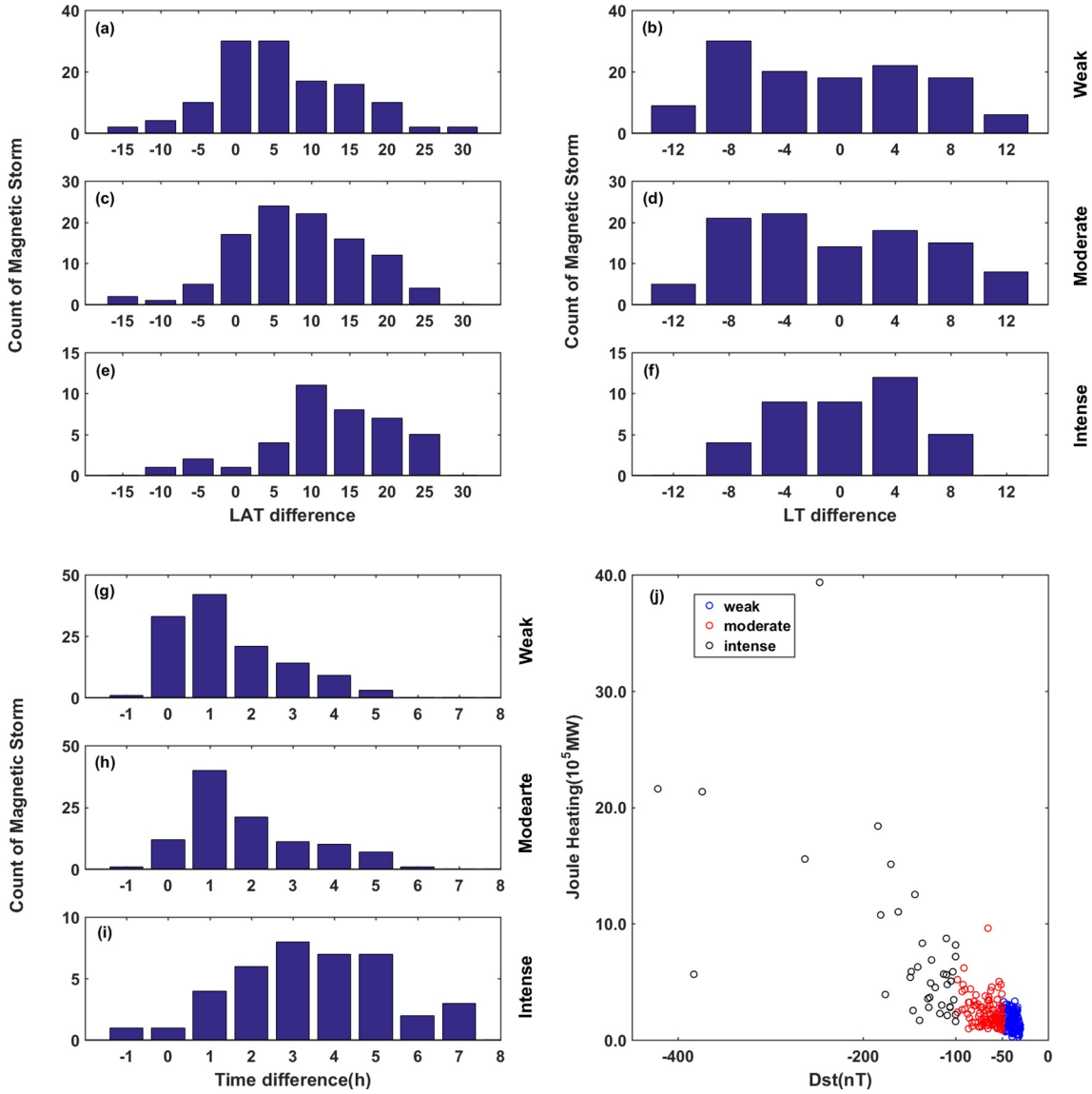

Figure 4. (top left column) Latitude difference, (top right column) LT difference, and (bottom left column) time difference between peak Joule heating and peak thermospheric density enhancement during (a, b, g) weak, (c, d, h) moderate, and (e, f, i) intense geomagnetic storms from 265 geomagnetic storm cases. (bottom right column) Distribution of Joule heating versus Dst during weak, moderate, and intense storms. Positive latitude, LT, and time differences mean that density enhancement occurs at higher latitude, later local time, and lags longer time than Joule heating.

4.2. Statistics From 265 Geomagnetic Storms

From the case study of the storm event during November 20 and 21, 2003, we can find out the latitudinal and LT dependences of Joule heating and thermospheric density during the intense geomagnetic storm. To statistically analyze the neutral density responses to Joule heating, we demonstrate the latitude and LT differences between the peak density enhancement and peak Joule heating for 265 geomagnetic storm events, as shown in Figures 4a–4f. We also show the differences in the times when the peaks in the Joule heating and the thermospheric density enhancement in Figures 4g–4i and variation of Joule heating with Dst in Figure 4j. From Figures 4a–4e, we can find that the latitude differences for 90% of geomagnetic storms are positive, which indicates that strong Joule heating tends to result in the significant density enhancement at higher-latitude region. Joule heating can be stronger for higher negative Dst with geomagnetic storms intensifying (Figure 4j).

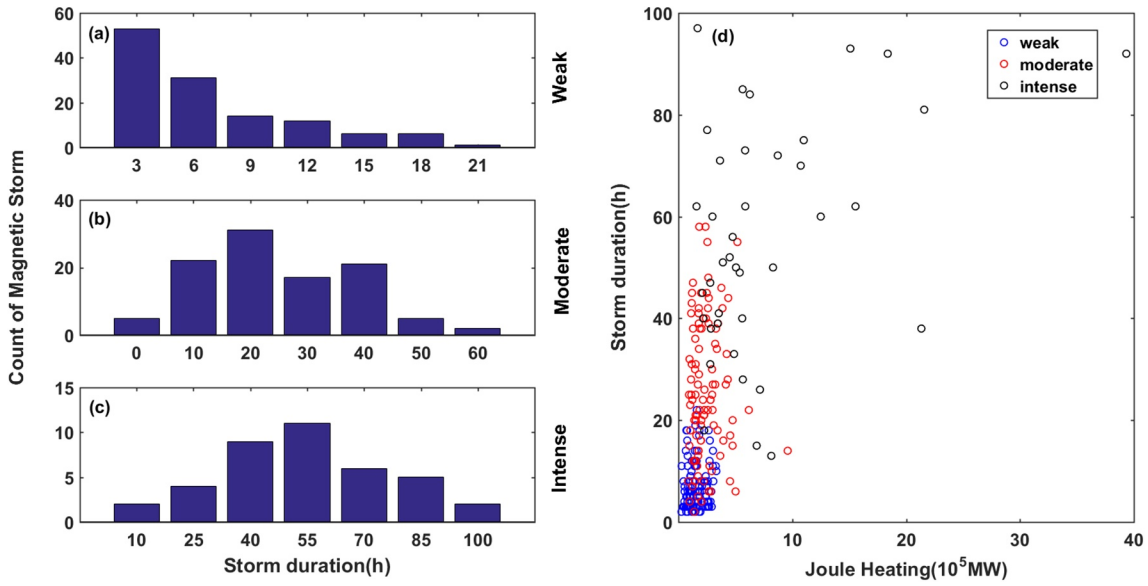

Figure 5. Storm duration during (a) weak, (b) moderate, and (c) intense geomagnetic storms from 265 geomagnetic storm cases. (d) Distribution of storm duration versus Joule heating during (blue) weak, (red) moderate, and (black) intense storms.

As shown in Figures 4a, 50% of weak geomagnetic storm cases involve the thermospheric density enhancement peaking in higher latitudes than the peak Joule heating about 0°–5° in latitudes. Figure 4c shows that 45% of moderate geomagnetic storm cases involve the density enhancement peaking in higher latitudes than peak Joule heating about 5°–10°, while it is about 10°–15° for 50% of intense geomagnetic storm cases in Figure 4e. In other words, Joule heating has the poleward influence on thermospheric density and such influence shifts to higher latitudes as storm intensity increases. In addition, during moderate and weak geomagnetic storms (Figures 4g and 4h), the time difference between Joule heating and the density enhancement is concentrated on 0–2 h, while for intense storms it is about 3–5 h (Figure 4i). The time differences follow the similar statistical trend to the latitude differences. As geomagnetic storms intensify, the increasing time differences may lead to increasing observed latitude differences. We will discuss the cause of the latitude difference is the longer time taken for the Joule heating (which tends to impact lower altitudes for more intense events) to affect the thermospheric density in Section 5.

Figures 4b–4f show the LT difference between the peak thermospheric density enhancement and peak Joule heating for weak, moderate, and intense geomagnetic storms. In Figures 4b and 4d, 87% of weak and moderate geomagnetic storm cases show LT differences about −8 to 8 LT. About 79% of intense storm cases involve LT difference about −4 to 4 LT (Figure 4f), which is smaller than that during moderate and weak storms. Wang, Miao, Aa, et al. (2020) have discovered that the correlation between thermospheric density and Joule heating is stronger for more intense geomagnetic storms. As geomagnetic storms intensify, thermospheric density is mainly affected by Joule heating, leading to density enhancement closer to Joule heating with LT, compared with weak storms. As a result, Joule heating can lead to the thermospheric density enhancement at higher latitudes, and the peak density enhancement in LT is closer to peak Joule heating as storm intensifies.

Geomagnetic storms vary not only in strength, but also in length. We show the durations of 265 geomagnetic storms in Figures 5a–5c and distribution of storm durations with Joule heating in Figure 5d for weak, moderate, and intense geomagnetic storms. In this study, we have defined Dst > −30 nT as the quiet time for geomagnetic storm. Thus, we calculate the storm durations between the times when Dst > −30 nT before and after the geomagnetic storms. As shown in Figures 5a–5c, the storm duration is concentrated on about 3–6 h for weak storms, 10–40 h for moderate storms, and 40–85 h for intense storms, which indicates that geomagnetic storms can last for longer time as the intensity of storm increases. From Figure 5d, storm duration increases with Joule heating. As geomagnetic storms intensify, Joule heating can be stronger, which increases thermospheric density in the high latitude regions. Due to the large-scale gravity waves and wind

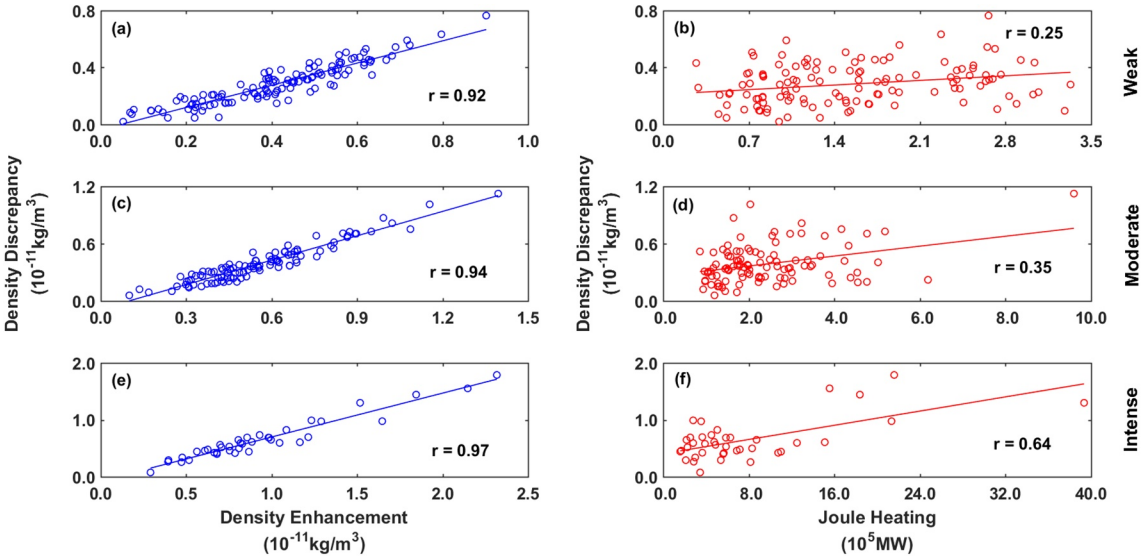

Figure 6. Peak thermospheric density discrepancy between observation and NRLMSISE-00 model versus the peak density enhancement (left column), and peak total Joule heating (right column) for weak (a, b), moderate (c, d), and intense geomagnetic storms (e, f) from 265 geomagnetic storms cases. The blue and red lines are the fitted results.

surges, the thermosphere circulates and leads to the global thermospheric density disturbance. Meanwhile, the increasing density can be ionized and decomposed to the plasma, which can lead to the conductance with Equation 1, contributing to the Joule heating (ΣpE2). As a result, Joule heating can last and extend the geomagnetic storm for the longer time with storm intensifying. Thus, due to strengthened energy injection, the geomagnetic storm can last for a longer time.

As outlined in Section 3 for an intense geomagnetic storm case, the increasing Joule heating causes thermospheric density to enhance, which leads to the increasing underestimation of the NRLMSISE-00 model, especially at high latitudes. We also analyze 265 geomagnetic storm events to statistically investigate the relation of the thermospheric density discrepancy with Joule heating. Figure 6 shows the scatterplot and linear regression between peak density discrepancy and peak density enhancement, and between peak density discrepancy and peak total Joule heating, for weak, moderate, and intense geomagnetic storms. From Figures 6a–6e, it is seen that thermospheric density discrepancy median increases from 0.4×10^{-11} to 1.0×10^{-11} kg/m^3 corresponding to density enhancement from 0.5×10^{-11} to 1.25×10^{-11} kg/m^3. This indicates that peak density discrepancy increases with the peak density enhancement as geomagnetic storms intensify. We calculate the correlation coefficient (r) between density discrepancy and density enhancement. They are 0.92 and 0.94 for weak and moderate geomagnetic storms, and 0.97 for intense geomagnetic storms. The positive correlation between density discrepancy and enhancement is well established during geomagnetic storms.

As shown in Figures 6b–6f, total Joule heating median also increases from 1.75×10^5 to 20.0×10^5 MW, which indicates that thermospheric density discrepancy increases with total Joule heating as storm intensifies. The correlation coefficient (r) between density discrepancy and total Joule heating is 0.25 and 0.35 for weak and moderate geomagnetic storms, while that for intense geomagnetic storms is 0.64. In this study, as we used the statistical patterns to calculate the Joule heating, the peak value of Joule heating may underestimate the maximum of actual Joule heating during geomagnetic storms. Besides, only based on the thermospheric density data from satellites passing by, the actual density discrepancy maximum may be larger than the peak discrepancy in Figure 6. However, the uncertainties for the peaks are negligible, the general accuracy of Figure 6 is reasonable. Thus, we can find that the correlation between density discrepancy and Joule heating is stronger as storm intensity increases.

The influence of Joule heating on thermospheric density discrepancy is weaker during weak and moderate geomagnetic storms, while it is stronger for intense geomagnetic storms. It has been found that Joule

Table 1
Latitudinal Distributions of Joule Heating and Density

Different geomagnetic storm magnitudes	Peak Joule heating (median location)	Peak thermospheric density enhancement (median location)
Weak	70.5°	77.9°
Moderate	68.3°	79.8°
Intense	68.0°	83.2°
Total storms	69.5°	78.2°

heating dominates the energy input for more intense storms by Wilson et al. (2006) and Knipp et al. (2004). Joule heating has a stronger influence on thermospheric density to enhance as the impact on storms intensifies. In addition, the correlation between density discrepancy and enhancement is strengthened, thus, Joule heating affects density discrepancy stronger. For the weaker geomagnetic storms, the other factors can also contribute to thermospheric density, such as neutral winds (Billett et al., 2018) and nitric oxide (NO) density (Knipp et al., 2017; Zesta & Oliveira, 2019; Y. Zhang et al., 2019). Thus, the correlation between density discrepancy and Joule heating is strengthened with storm intensity increasing. In consequence, as geomagnetic storms intensify, Joule heating has a stronger impact on thermospheric density discrepancy between observation and NRLMSISE-00 model.

5. Summary and Discussion

From 265 geomagnetic storm cases from 2002 to 2008, we statistically investigate Joule heating and the response of high-latitude thermospheric density, which shows density discrepancies between observations and simulations. First, during geomagnetic storms, Joule heating can cause the thermospheric density to increase at higher latitudes. Second, during moderate and weak geomagnetic storms, the latitude differences between the peak Joule heating and the peak density enhancement are 0°–5° and 5°–10° in latitude, while for the intense storms, the latitude differences increase to 10°–15°. Third, the LT difference is −8 to 8 LT during weak and moderate geomagnetic storms, and −4 to 4 LT during intense storms. Finally, the correlation between density discrepancy and total Joule heating is stronger as storm intensity increases.

During geomagnetic storms, the impacts of Joule heating on thermospheric density extend to higher-latitude regions. Using the observed neutral wind variations driven by subauroral polarization streams (SAPS) (Foster & Burke, 2002) where strong ion drag cause a westward neutral wind (Wang et al., 2012), S.-R. Zhang et al. (2015) found that the poleward Coriolis force effects on the westward wind can establish a poleward wind surge during the geomagnetic storm. The poleward wind surge can be seen as traveling atmosphere disturbances (TADs) in the high-latitude thermosphere (Shiokawa et al., 2003). Consequently, the heated thermospheric density by local Joule heating can transfer to the higher latitudes through TADs due to the poleward wind.

During intense geomagnetic storms, the differences in the latitude corresponding to Joule heating with the latitudes where high-latitude densities enhance are larger than that those during moderate and weak geomagnetic storms. We suggest that this results from various responding times of thermospheric density at 400 km to Joule heating during different storm magnitudes. As geomagnetic activity intensifies, Joule heating deposits at lower altitudes (Cheng et al., 2017; Wu et al., 2020), needing more time to conduct upward to the thermosphere (Huang et al., 2012). From Figures 4g to 4i, we also found that the responding time of thermospheric density at 400 km to Joule heating is longer as storm intensity increases. The responding time follows the similar statistical trend to the latitude difference. As the heated thermospheric density transfers to higher latitudes due to the poleward wind, the density propagation is allowed to take a longer time thus influences more poleward regions for more intense geomagnetic storms.

We also analyze the latitudinal distributions of the peak Joule heating, as well as the peak thermospheric density enhancement during different geomagnetic storm magnitudes in Table 1. During geomagnetic storms, the median location of peak Joule heating is concentrated on about 70° in latitude. As for the peak density median location, it is 77.9° and 79.8° during weak and moderate storms, while it increases to 83.2° for intense storms. We can find that the thermospheric density location occurs at relatively higher latitudes as storm intensity increases. As a result, when Joule heating affects the thermospheric density at 400 km via upwelling (Lühr et al., 2004; Wu et al., 2020) and such effect maximizes as geomagnetic storms intensify, the local density has transferred poleward for a longer time and reached the polar region for a longer distance simultaneously.

In this study, we ignore the inputs from the neutral wind when calculating the Joule heating (Lu et al., 1995). This may underestimate the effect of Joule heating. Billett et al. (2018) recently demonstrated that neutral winds play an important role in the morphology and output of Joule heating. Exploring the Joule heating and its influences on thermospheric density may make a slight error for the study by ignoring the neutral wind. Further study will take neutral wind into account to obtain Joule heating.

Our study of Joule heating impacts on high-latitude thermospheric density during geomagnetic storm cases reveals a sequence of poleward impacts on storm-time density. The statistical results provide a valuable database for empirical and physical models to resolve neutral densities during different levels of storms. To better understand the physical and dynamical processes that establish the relation between Joule heating and thermospheric densities, including their latitudinal and LT distributions, numerical modeling efforts are desirable in the future study.

Data Availability Statement

The authors obtain the DSMP data and ACE data from https://cdaweb.gsfc.nasa.gov/index.html/ and https://omniweb.gsfc.nasa.gov/. CHAMP data and GRACE data are from https://isdc.gfzpotsdam.de/ at the website of the Information System and Data Center in Postdam, Germany. The solar flux proxy, F10.7, is obtained from https://omniweb.gsfc.nasa.gov/form/dx1.html and the disturbance storm time index, Dst, is obtained from http://wdc.kugi.kyoto-u.ac.jp/. The NRLMSISE-00 and Weimer model are from https://ccmc.gsfc.nasa.gov/.

Acknowledgments
This study is supported by the Strategic Priority Research Program of Chinese Academy of Sciences (XDA17010302) and the National Science Foundation of China (41674183 and 41974184).

References

Barth, C. A., Lu, G., & Roble, R. G. (2009). Joule heating and nitric oxide in the thermosphere. *Journal of Geophysical Research: Space Physics*, *114*(A5). https://doi.org/10.1029/2008ja013765

Billett, D. D., Grocott, A., Wild, J. A., Walach, M. T., & Kosch, M. J. (2018). Diurnal variations in global Joule heating morphology and magnitude due to neutral winds. *Journal of Geophysical Research: Space Physics*. *123*(3), 2398–2411. https://doi.org/10.1002/2017ja025141

Buonsanto, M. J. (1999). Ionospheric storms—A review. *Space Science Reviews*, *88*(3), 563–601. https://doi.org/10.1023/a:1005107532631

Cheng, S., Yue, D., Yang, L., & Yue, X. (2017). Dependence of Pedersen conductance in the E and F regions and their ratio on the solar and geomagnetic activities. *Space Weather*, *15*(3), 484–494.

Crowley, G., Knipp, D. J., Drake, K. A., Lei, J., Sutton, E., & Lühr, H. (2010). Thermospheric density enhancements in the dayside cusp region during strong BY conditions. *Geophysical Research Letters*, *37*, L07110. https://doi.org/10.1029/2009GL042143

Deng, Y., Fuller-Rowell, T. J., Ridley, A. J., Knipp, D., & Lopez, R. E. (2013). Theoretical study: Influence of different energy sources on the cusp neutral density enhancement. *Journal of Geophysical Research - A: Space Physics*, *118*, 2340–2349. https://doi.org/10.1002/jgra.50197

Deng, Y., Huang, Y., Lei, J., Ridley, A. J., Lopez, R., & Thayer, J. (2011). Energy input into the upper atmosphere associated with high-speed solar wind streams in 2005. *Journal of Geophysical Research Space Physics*, *116*(A5). https://doi.org/10.1029/2010ja016201

Doornbos, E., & Klinkrad, H. (2006). Modeling of space weather effects on satellite drag. *Advances in Space Research*, *37*(6), 1229–1239. https://doi.org/10.1016/j.asr.2005.04.097

Emmert, J. T. (2015). Thermospheric mass density: A review. *Advances in Space Research*, *56*(5), 773–824. https://doi.org/10.1016/j.asr.2015.05.038

Fedrizzi, M., Fuller-Rowell, T. J., & Codrescu, M. V. (2012). Global Joule heating index derived from thermospheric density physics-based modeling and observations. *Space Weather*, *10*, S03001. https://doi.org/10.1029/2011SW000724

Forbes, J. M., & Roble, R. G. (1990). Thermosphere-ionosphere coupling: An experiment in interactive modeling. *Journal of Geophysical Research*, *95*(A1), 201. https://doi.org/10.1029/JA095iA01p00201

Foster, J. C., & Burke, W. J. (2002). SAPS: A new characterization for sub-auroral electric fields. *Eos, Transactions American Geophysical Union*, *83*(36), 393. https://doi.org/10.1029/2002EO000289

Fuller-Rowell, T. J., Codrescu, M. V., Moffett, R. J., & Quegan, S. (1994). Response of the thermosphere and ionosphere to geomagnetic storms. *Journal of Geophysical Research*, *99*(A3), 3893–3914. https://doi.org/10.1029/93JA02015

Gonzalez, W. D., Tsurutani, B. T., & Gonzalez, A. L. C. D. (1999). Interplanetary origin of geomagnetic storms. *Space Science Reviews*, *88*(3–4), 529–562. https://doi.org/10.1023/a:1005160129098

Hagan, M. E., & Sipler, D. P. (1991). Combined incoherent scatter radar and Fabry-Perot interferometer measurements of frictional heating effects over Millstone Hill during March 7–10, 1989. *Journal of Geophysical Research*, *96*(A1), 289–296. https://doi.org/10.1029/90JA02250

Hardy, D. A., Gussenhoven, M. S., Raistrick, R., & Mcneil, W. J. (1987). Statistical and functional representations of the pattern of auroral energy flux and conductivity. *Journal of Geophysical Research Space Physics*, *92*(A11), 12275–12294. https://doi.org/10.1029/ja092ia11p12275

Hedin, A. E. (1987). MSIS-86 thermospheric model. *Journal of Geophysical Research*, *92*(A5), 4649–4662. https://doi.org/10.1029/ja092ia05p04649

Hedin, A. E. (1991). Extension of the MSIS thermosphere model in the middle and lower atmosphere. *Journal of Geophysical Research Space Physics*, *96*(A2), 1159–1172. https://doi.org/10.1029/90ja02125

Huang, Y., Richmond, A. D., Yue, D., & Roble, R. (2012). Height distribution of Joule heating and its influence on the thermosphere. *Journal of Geophysical Research Space Physics*, *117*(A8), 8334. https://doi.org/10.1029/2012ja017885

Jacchia, L. G. (1971). New static models of the thermosphere and exosphere with empirical temperature profiles. *SAO Special Report*, *313*(20), 3138–3144.

Knipp, D. J., Pette, D. V., Kilcommons, L. M., Isaacs, T. L., Cruz, A. A., Mlynczak, M. G., et al. (2017). Thermospheric nitric oxide response to shock-led storms. *Space Weather*, *15*(2), 325–342. https://doi.org/10.1002/2016SW001567

Knipp, D. J., Tobiska, W. K., & Emery, B. A. (2004). Direct and indirect thermospheric heating sources for solar cycles 21-23. *Solar Physics*, *224*(1), 495–505. https://doi.org/10.1007/s11207-005-6393-4

Krauss, S., Temmer, M., & Vennerstrom, S. (2018). Multiple satellite analysis of the Earth's thermosphere and interplanetary magnetic field variations due to ICME/CIR events during 2003-2015. *Journal of Geophysical Research-Space Physics*, *123*(10), 8884–8894. https://doi.org/10.1029/2018ja025778

Lei, J., Thayer, J. P., Forbes, J. M., Sutton, E. K., Nerem, R. S., Temmer, M., & Veronig, A. M. (2008). Global thermospheric density variations caused by high-speed solar wind streams during the declining phase of solar cycle 23. *Journal of Geophysical Research*, *113*, A11303. https://doi.org/10.1029/2008JA013433

Liu, H., & Lühr, H. (2005). Strong disturbance of the upper thermospheric density due to magnetic storms: CHAMP observations. *Journal of Geophysical Research*, *110*, A09S29. https://doi.org/10.1029/2004JA010908

Liu, H., Lühr, H., & Watanabe, S. (2007). Climatology of the equatorial thermospheric mass density anomaly. *Journal of Geophysical Research*, *112*, A05305. https://doi.org/10.1029/2006JA012199

Lu, G., Richmond, A. D., Emery, B. A., & Roble, R. G. (1995). Magnetosphere-ionosphere-thermosphere coupling: Effect of neutral winds on energy transfer and field-aligned current. *Journal of Geophysical Research*, *100*(A10), 19643–19659. https://doi.org/10.1029/95JA00766

Lu, G., Richmond, A. D., Lühr, H., & Paxton, L. (2016). High-latitude energy input and its impact on the thermosphere. *Journal of Geophysical Research-Space Physics*, *121*(7), 7108–7124. https://doi.org/10.1002/2015ja022294

Lühr, H., & Marker, S. (2013). High-latitude thermospheric density and wind dependence on solar and magnetic activity. In F.-J. Lübken (Eds.), *Climate and Weather of the Sun-Earth System (CAWSES): Highlights from a priority program* (pp. 189–205). Springer. https://doi.org/10.1007/978-94-007-4348-9_11

Lühr, H., Rother, M., Köhler, W., Ritter, P., & Grunwaldt, L. (2004). Thermospheric up-welling in the cusp region: Evidence from CHAMP observations. *Geophysical Research Letters*, *31*, 6805. https://doi.org/10.1029/2003GL019314

Miao, J., Liu, S., Zhitao, L. I., Huang, W., & Tang, G. (2012). Correlation of thermosphere density variation with different solar and geomagnetic indices. *Manned Spaceflight*, *18*(5), 24–30. https://doi.org/10.16329/j.cnki.zrht.2012.05.001

Oliveira, D. M., & Zesta, E. (2019). Satellite orbital drag during magnetic storms. *Space Weather*, *17*(11), 1510–1533. https://doi.org/10.1029/2019sw002287

Picone, J. M., Hedin, A. E., Drob, D. P., & Aikin, A. C. (2002). NRL-MSISE-00 empirical model of the atmosphere: Statistical comparisons and scientific issues. *Journal of Geophysical Research*, *107*(A12), SIA15-1–SIA15-16. https://doi.org/10.1029/2002ja009430

Prölss, G. W. (2011). Density perturbations in the upper atmosphere caused by the dissipation of solar wind energy. *Surveys in Geophysics*, *32*(2), 101–195. https://doi.org/10.1007/s10712-010-9104-0

Redmon, R. J., Denig, W. F., Kilcommons, L. M., & Knipp, D. J. (2017). New DMSP database of precipitating auroral electrons and ions. *Journal of Geophysical Research: Space Physics*, *122*, 9056–9067. https://doi.org/10.1002/2016JA023339

Reigber, C., Lühr, H., & Schwintzer, P. (2002). CHAMP mission status. *Advances in Space Research*, *30*(2), 129–134. https://doi.org/10.1016/s0273-1177(02)00276-4

Rentz, S. (2009). *The upper atmospheric fountain effect in the polar cusp region* (Ph.D. Thesis).

Richmond, A. D., & Lu, G. (2000). Upper-atmospheric effects of magnetic storms: A brief tutorial. *Journal of Atmospheric and Solar-Terrestrial Physics*, *62*(12), 1115–1127. https://doi.org/10.1016/s1364-6826(00)00094-8

Rishbeth, H. (1977). Drifts and winds in the polar F region. *Journal of Atmospheric and Terrestrial Physics*, *39*(1), 111–116. https://doi.org/10.1016/0021-9169(77)90051-4

Robinson, R. M., Vondrak, R., Miller, K., Dabbs, T., & Hardy, D. (1987). On calculating ionospheric conductances from the flux and energy of precipitating electrons. *Journal of Geophysical Research*, *92*(A3), 2565–2569. https://doi.org/10.1029/ja092ia03p02565

Robinson, R. M., & Vondrak, R. R. (1984). Measurements of E region ionization and conductivity produced by solar illumination at high latitudes. *Journal of Geophysical Research Space Physics*, *89*(A6), 3951–3956. https://doi.org/10.1029/ja089ia06p03951

Shi, Y., Zesta, E., Connor, H. K., Su, Y.-J., Sutton, E. K., Huang, C. Y., et al. (2017). High-latitude thermosphere neutral density response to solar wind dynamic pressure enhancement. *Journal of Geophysical Research: Space Physics*, *122*(11), 11559–11578. https://doi.org/10.1002/2017JA023889

Shiokawa, K., Otsuka, Y., Ogawa, T., Kawamura, S., Yamamoto, M., Fukao, S., et al. (2003). Thermospheric wind during a storm-time large-scale traveling ionospheric disturbance. *Journal of Geophysical Research*, *108*(A12), 1423. https://doi.org/10.1029/2003JA010001

Srivastava, N., & Venkatakrishnan, P. (2004). Solar and interplanetary sources of major geomagnetic storms during 1996-2002. *Journal of Geophysical Research*, *109*(A10). https://doi.org/10.1029/2003ja010175

Sutton, E. K., Forbes, J. M., & Knipp, D. J. (2009). Rapid response of the thermosphere to variations in Joule heating. *Journal of Geophysical Research*, *114*, A04319. https://doi.org/10.1029/2008JA013667

Tapley, B. D., Bettadpur, S., Watkins, M., & Reigber, C. (2004). The gravity recovery and climate experiment: Mission overview and early results. *Geophysical Research Letters*, *31*(9). https://doi.org/10.1029/2004gl019920

Thayer, J. P., Lei, J., Forbes, J. M., Sutton, E. K., & Nerem, R. S. (2008). Thermospheric density oscillations due to periodic solar wind high-speed streams. *Journal of Geophysical Research*, *113*, A06307. https://doi.org/10.1029/2008JA013190

Vickrey, J. F., Vondrak, R. R., & Matthews, S. J. (1982). Energy deposition by precipitating particles and Joule dissipation in the auroral ionosphere. *Journal of Geophysical Research*, *87*, 5184–5196. https://doi.org/10.1029/ja087ia07p05184

Wang, W., Talaat, E. R., Burns, A. G., Emery, B., Hsieh, S., Lei, J., & Xu, J. (2012). Thermosphere and ionosphere response to subauroral polarization streams (SAPS): Model simulations. *Journal of Geophysical Research*, *117*, A07301. https://doi.org/10.1029/2012JA017656

Wang, X., Miao, J., Aa, E., Ren, T., Wang, Y., Liu, J., & Liu, S. (2020). Statistical analysis of Joule heating and thermosphere response during geomagnetic storms of different magnitudes. *Journal of Geophysical Research: Space Physics*, *125*, e2020JA027966. https://doi.org/10.1029/2020JA027966

Wang, X., Miao, J., Liu, S. Q., & Ren, T. L. (2020). Characteristics analysis of thermospheric density response during the different intensity of geomagnetic storms. *Chinese Journal of Space Science*, *40*(1), 28–41.

Weimer, D. R. (2001). An improved model of ionospheric electric potentials including substorm perturbations and application to the Geospace Environment Modeling November 24, 1996, event. *Journal of Geophysical Research Space Physics*, *106*(A1), 407–416. https://doi.org/10.1029/2000ja000604

Wilson, G. R., Weimer, D. R., Wise, J. O., & Marcos, F. A. (2006). Response of the thermosphere to Joule heating and particle precipitation. *Journal of Geophysical Research Space Physics*, *111*(A10). https://doi.org/10.1029/2005ja011274

Wu, H., Lu, X., Lu, G., Chu, X., Wang, W., Yu, Z., et al. (2020). Importance of regional-scale auroral precipitation and electrical field variability to the storm-time thermospheric temperature enhancement and inversion layer (TTEIL) in the Antarctic E region. *Journal of Geophysical Research: Space Physics*, *125*, e2020JA028224. https://doi.org/10.1029/2020ja028224

Xu, J., Wang, W., Lei, J., Sutton, E. K., & Chen, G. (2011). The effect of periodic variations of thermospheric density on CHAMP and GRACE orbits. *Journal of Geophysical Research*, *116*, A02315. https://doi.org/10.1029/2010JA015995

Xu, J., Wang, W., Zhang, S., Liu, X., & Yuan, W. (2015). Multiday thermospheric density oscillations associated with variations in solar radiation and geomagnetic activity. *Journal of Geophysical Research Space Physics*, *120*, 3829–3846. https://doi.org/10.1002/2014JA020830

Zesta, E., & Huang, C. Y. (2016). Satellite orbital drag. In G. V. Khazanov (Ed.), *Space weather fundamentals* (pp. 329–351). CRC Press. https://doi.org/10.1201/9781315368474-20

Zesta, E., & Oliveira, D. M. (2019). Thermospheric heating and cooling times during geomagnetic storms, including extreme events. *Geophysical Research Letters*, *46*(22), 739–12746. https://doi.org/10.1029/2019GL085120

Zhang, B., Lotko, W., Brambles, O., Wiltberger, M., Wang, W., Schmitt, P., & Lyon, J. (2012). Enhancement of thermospheric mass density by soft electron precipitation. *Geophysical Research Letters*, *39*, L20102. https://doi.org/10.1029/2012GL053519

Zhang, S.-R., Erickson, P. J., Foster, J. C., Holt, J. M., Coster, A. J., Makela, J. J., et al. (2015). Thermospheric poleward wind surge at midlatitudes during great storm intervals. *Geophysical Research Letters*, *42*, 5132–5140. https://doi.org/10.1002/2015GL064836

Zhang, Y., Paxton, L. J., Lu, G., & Yee, S. (2019). Impact of nitric oxide, solar EUV and particle precipitation on thermospheric density decrease. *Journal of Atmospheric and Solar-Terrestrial Physics*, *182*, 147–154. https://doi.org/10.1016/j.jastp.2018.11.016